Effect on the divertor and scrape-off layer plasma properties of the distribution of power and particle influxes from the core

W. M. Stacey[a)]
Georgia Institute of Technology, Atlanta, Georgia 30332, USA

(Received 30 October 2008; accepted 12 February 2009; published online 25 March 2009)

Calculations of the profiles along the field lines within the divertor and scrape-off layer (SOL) of differences in the plasma ion density, temperature, parallel current, parallel flow velocity, and electrostatic potential, which result from using different poloidal distributions of the particle and heat influxes crossing the separatrix from the core plasma into the SOL, are presented and discussed vis-à-vis experimental observations. The calculations show that the stronger outboard than inboard particle and heat fluxes into the SOL caused by the geometric compression/expansion of flux surfaces predicted by magnetohydrodynamic equilibrium calculations lead to a prediction of higher plasma temperature at the outboard divertor than at the inboard divertor, a result that is consistent with experimental observation and that confirms a previous prediction (made without accounting for drifts) of a possible cause of the observed in-out divertor power asymmetry. The calculations also illustrate the effect of the poloidal distribution of particle and power influx into the SOL on the flow velocity, parallel current, and electrostatic potential distributions in the SOL and divertor. © *2009 American Institute of Physics*. [DOI: 10.1063/1.3094856]

I. INTRODUCTION

Although it stands to reason that the poloidal distribution of the heat and particle influxes crossing the separatrix from the core of a tokamak plasma into the scrape-off layer (SOL) will affect the parallel profiles of the density, temperature, flows, etc., within the SOL and divertor, the poloidal variation over the last-closed-flux surface (LCFS) of these influxes is frequently treated quite approximately. In simple models, the influxes across the LCFS into the SOL may be taken as poloidally uniform when calculating SOL and divertor plasma conditions. Even in more sophisticated edge calculations, the particle and power fluxes from the core across the inner boundary of the edge of the computation domain (which is somewhat inside the LCFS) may be assumed to be poloidally uniform (e.g., Ref. 1). In any case, it is of interest to examine the effect of using poloidally dependent particle and heat influxes across the LCFS, determined by the magnetohydrodynamic (MHD) equilibrium conditions, instead of uniform influxes, on the calculation of plasma profiles in the SOL and divertor, which is the purpose of this paper. We note that a similar investigation of the effect of poloidally dependent heat and particle influxes on the in-out divertor power asymmetry has previously been performed,[2] but without taking into account the effects of $E \times B$ and diamagnetic drifts.

If the heat flux crossing the separatrix from the core into the SOL was purely conductive (i.e., proportional to the temperature gradient normal to the flux surface), then the assumption that the poloidal dependence of the heat flux was inversely proportional to the poloidal dependence of the distance between flux surfaces would be plausible, and this separation of flux surfaces could be calculated from MHD equilibrium theory. We have made a number of calculations[3] which indicate that, at least in DIII-D,[4] the heat flux crossing the separatrix from the plasma core into the SOL is largely conductive, which encourages the use of a MHD calculation of (the inverse of) the poloidal dependence of the separation between flux surfaces to model the poloidal dependence of the heat flux crossing the separatrix from the core into the SOL.

The justification for using (the inverse of) the poloidal dependence of the separation between flux surfaces to model the poloidal dependence of the particle influx crossing the separatrix from the core into the SOL would follow immediately if the particle influx was diffusive (i.e., proportional to the density gradient). Note that the assumption of constant (in real space) transport coefficients and purely diffusive transport made in Ref. 2 would lead to the same model. Moreover, a diffusive model, together with an inward particle pinch, is generally found to provide a reasonable fit to edge density profiles, and there is some theoretical and experimental justification[5,6] for such a model. The implication of such a model is a very large diffusive component of the particle flux, so the same poloidal dependence will be used for the particle and heat fluxes.

This paper is structured as follows. The model for the poloidal dependence of the particle and heat fluxes crossing the separatrix from the core into the SOL is described in Sec. II, then the computational model for the divertor and SOL plasma is reviewed in Sec. III. The density, temperature, flow velocity, etc., profiles in the divertor and SOL calculated for a model problem based on DIII-D discharge parameters, with (i) uniform incident particle and heat fluxes from the core and (ii) poloidally dependent particle and heat fluxes, are compared in Sec. IV. The work is summarized in Sec. V.

[a)]Electronic mail: weston.stacey@nre.gatech.edu.

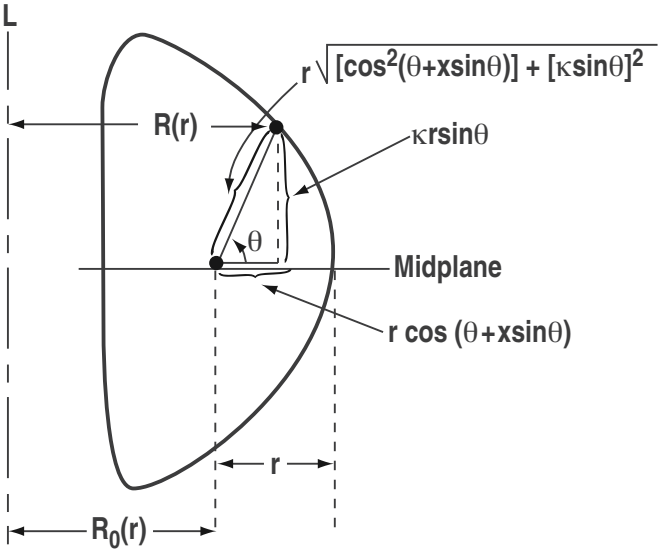

FIG. 1. Miller model equilibrium geometric parameters.

II. POLOIDAL DISTRIBUTION OF THE HEAT AND PARTICLE FLUXES

A. Miller equilibrium

While the poloidal distribution of the separation between flux surfaces can be calculated numerically by solving the Grad–Shafranov equation, it is more convenient to make use of the analytical expressions derived by Miller *et al.*[7] for an equilibrium flux surface in a plasma as shown in Fig. 1 with elongation κ, triangularity δ, and displaced centers $R_0(r)$, where r is the half-diameter of the plasma along the midplane with center located at distance $R_0(r)$ from the toroidal centerline.

The R and Z coordinates of this plasma are described by[7]

$$R(r) = R_0(r) + r\cos[\theta + x\sin\theta] \equiv R_0(r) + r\cos\xi,$$
$$Z(r) = \kappa r\sin\theta, \tag{1}$$

where $x \equiv \sin^{-1}\delta$.

The poloidal magnetic field in such flux surface geometry is[7]

$$RB_p = |\nabla\phi\times\nabla\psi| = \frac{\partial\psi}{\partial r}|\nabla r| = \frac{\frac{\partial\psi}{\partial r}\kappa^{-1}[\sin^2(\theta+x\sin\theta)(1+x\cos\theta)^2+\kappa^2\cos^2\theta]^{1/2}}{\cos(x\sin\theta)+\frac{\partial R_0}{\partial r}\cos\theta+[s_\kappa - s_\delta\cos\theta+(1+s_\kappa)x\cos\theta]\sin\theta\sin(\theta+x\sin\theta)}, \tag{2}$$

where $s_\kappa = (r/\kappa)(\partial\kappa/\partial r)$ and $s_\delta = r(\partial\delta/\partial r)/\sqrt{(1-\delta^2)}$ account for the change in elongation and triangularity, respectively, with radial location.

The shifted circle model (which leads to the Shafranov shift) yields[7]

$$\frac{\partial R_0}{\partial r} \equiv \Delta' = -\frac{r}{R_0}\left(\beta_p + \frac{1}{2}\ell_i\right). \tag{3}$$

Here $\beta_p = nT/(B_\theta^2/2\mu_0)$ and ℓ_i is the internal inductance.

The flux surface average (FSA) of a quantity $A(r,\theta)$ in this flux surface geometry is

$$\langle A(r,\theta)\rangle \equiv \frac{\oint\frac{A(r,\theta)d\ell_p}{B_p}}{\oint\frac{d\ell_p}{B_p}} = \frac{\oint A(r,\theta)z(r,\theta)d\ell_p}{\oint z(r,\theta)d\ell_p}, \tag{4}$$

where

$$z(r,\theta) \equiv \frac{\cos(x\sin\theta)+\frac{\partial R_0}{\partial r}\cos\theta+[s_\kappa - s_\delta\cos\theta+(1+s_\kappa)x\cos\theta]\sin\theta\sin(\theta+x\sin\theta)}{[\sin^2(\theta+x\sin\theta)(1+x\cos\theta)^2+\kappa^2\cos^2\theta]^{1/2}/[R_0(r)+r\cos(\theta+x\sin\theta)]}, \tag{5}$$

and the differential poloidal length is (see Fig. 1)

$$d\ell_p = r\sqrt{[\cos^2(\theta+x\sin\theta)+\kappa^2\sin^2\theta]}d\theta. \tag{6}$$

B. Poloidal dependence of heat flux

Assuming that the density and temperature are uniform over the flux surface, a poloidal dependence of the conductive heat flux must arise either through the poloidal dependence of the radial temperature gradient

$$q(r,\theta) = n(r)T(r)\chi(r)L_T^{-1}(r,\theta) = n(r)T(r)\chi(r)\langle L_T(r)\rangle^{-1}H(r,\theta) \quad (7)$$

or through a poloidal dependence of the underlying radial transport mechanism (e.g., turbulence[8]) that causes $\chi \sim \chi(r,\theta)$. In this paper we consider only the former geometric effect of flux surface expansion/compression and elongation.

The quantity $H(r,\theta) \equiv q(r,\theta)/\langle q(r)\rangle \equiv \langle L_T(r)\rangle / L_T(r,\theta)$ can be calculated[8] using the Miller equilibrium above. The local temperature gradient scale length can be related to the average value over the flux surface

$$\langle L_T\rangle = -T(dr/dT)_\theta[\langle dr\rangle/dr(\theta)] \equiv (L_T)_\theta[\langle dr\rangle/dr(\theta)] = (L_T)_\theta[|\nabla r(\theta)|/\langle|\nabla r|\rangle]. \quad (8)$$

From Eq. (2), the local $|\nabla r(\theta)|$ may be written as

$$|\nabla r(r,\theta)| = \frac{\kappa^{-1}[\sin^2(\theta + x\sin\theta)(1 + x\cos\theta)^2 + \kappa^2\cos^2\theta]^{1/2}}{\cos(x\sin\theta) + \frac{\partial R_0}{\partial r}\cos\theta + [s_\kappa - s_\delta\cos\theta + (1+s_\kappa)x\cos\theta]\sin\theta\sin(\theta + x\sin\theta)}. \quad (9)$$

Using this in Eq. (4) yields an expression for the FSA value

$$\langle|\nabla r(r)|\rangle = \frac{\int_0^{2\pi}[R_0(r) + r\cos(\theta + x\sin\theta)][\cos^2(\theta + x\sin\theta) + \kappa^2\sin^2\theta]^{1/2}d\theta}{\int_0^{2\pi}F(r,\theta)[R_0(r) + r\cos(\theta + x\sin\theta)][\cos^2(\theta + x\sin\theta) + \kappa^2\sin^2\theta]^{1/2}d\theta}, \quad (10)$$

where

$$F(r,\theta) = \frac{\cos(x\sin\theta) + \frac{\partial R_0}{\partial r}\cos\theta + [s_\kappa - s_\delta\cos\theta + (1+s_\kappa)x\cos\theta]\sin\theta\sin(\theta + x\sin\theta)}{\kappa^{-1}[\sin^2(\theta + x\sin\theta)(1 + x\cos\theta)^2 + \kappa^2\cos^2\theta]^{1/2}}. \quad (11)$$

The quantity $H(r,\theta)$ is then determined by

$$H(r,\theta) \equiv q(r,\theta)/\langle q(r)\rangle \equiv \langle L_T(r)\rangle/L_T(r,\theta) = |\nabla r(r,\theta)|/\langle|\nabla r(r)|\rangle. \quad (12)$$

Calculations of $H(r,\theta)$ based on these equations for a DIII-D discharge were in very good agreement[9] with calculations made by the two dimensional (2D) transport codes UEDGE (Ref. 10) and SOLPS (Ref. 11) using experimental data distributed over equilibrium fit flux surfaces calculated numerically using experimental data.

III. SOL AND DIVERTOR CALCULATION MODEL

In principle, the problem of solving for the flows, currents, densities, etc., in the SOL and divertor can be addressed by solving the full momentum and particle balance, current divergence, and other governing equations in the actual physical and magnetic geometry, without building in any prior knowledge of the nature of the solution. However, such an approach leads to practical difficulties.

One difficulty is that the resulting calculation of some important quantities is of the form of a small difference of two or more large terms, leading to numerical problems in achieving a solution. This has led previous workers[11] to manipulation of the equations involved to analytically eliminate the divergence-free terms in the particle and current balance equations. This work has shown that the non-divergence-free part of the large diamagnetic velocities is proportional to gradients in the magnetic field and represents the vertical guiding center drift of ions caused by ∇B. A second difficulty arises in the accurate evaluate of these magnetic gradient terms. Rognlien *et al.*[10] avoided this second difficulty by using analytical expressions for the divergence-free leading order diamagnetic and $E\times B$ drifts and then using analytical expressions for the higher order grad B and curvature drifts (rather than numerically differentiating the local magnetic field), thus avoiding the requirement for a very accurate representation of the local field geometry.

We have taken into account the experience of these two previous sets of authors[10,11] to formulate a simplified solution procedure for the parallel flows, currents, densities, etc., in the SOL and divertor. Specifically, we use the leading order divergence-free diamagnetic velocity to calculate particle flows, but use the analytical vertical grad B (and curvature) drift expression to account for the contribution of the diamagnetic flows to the divergence of the current, and we use a radial-poloidal geometry but with the poloidal component mapped onto a "pseudoparallel" coordinate to facilitate the calculation. We go beyond these previous authors to approximate the radial calculations in order to reduce the computational intensity of the calculation.

A. Geometrical model

The calculation is formulated in the "radial-poloidal" strip of plasma outside the separatrix shown in Fig. 2. For convenience in representing the divertor channels and for doing particle, energy, and momentum balances, the "poloidal" coordinate is mapped onto a pseudoparallel coordinate, ξ. The plasma outside the separatrix is modeled as a "stack"

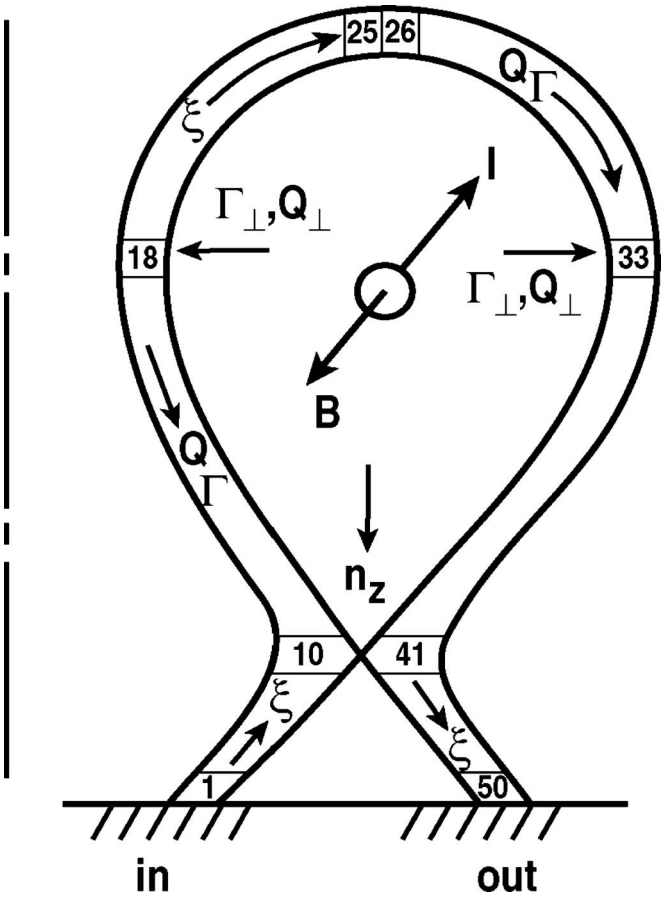

FIG. 2. SOL-divertor geometric model.

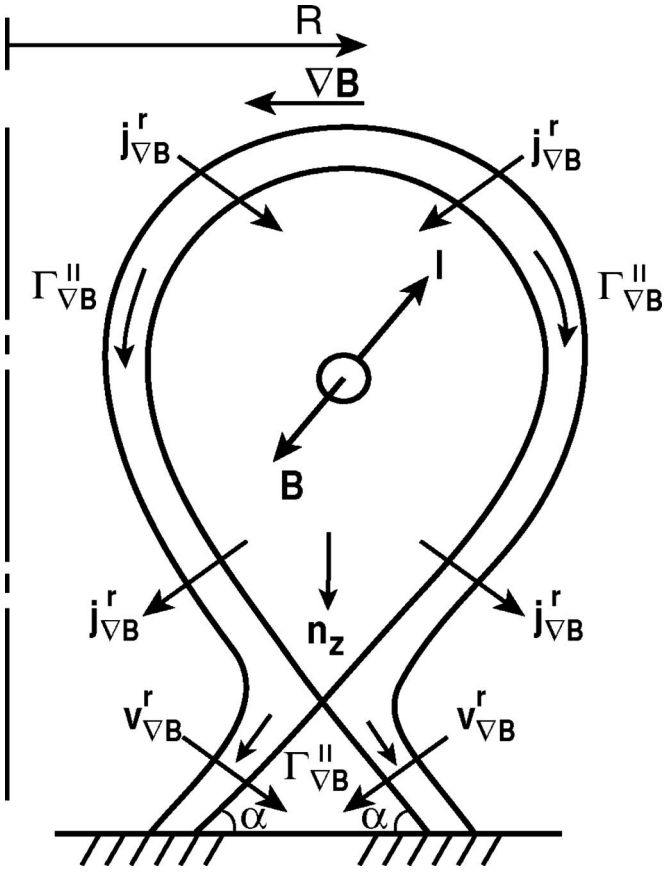

FIG. 3. grad B and curvature drifts.

of 2D strips, or "ribbons," that spiral about the core plasma (q times between X points) following the magnetic field lines from the inner to the outer divertor target plate. The effect of nonuniformities in the magnetic geometry are accounted for by particle "drifts" (see Fig. 3) to account for the effects of field gradients and curvature, while retaining a simple computational geometry. The parameter ξ designates the distance "along the field lines" from the inner ($\xi=\xi_{\rm in}$) to the outer ($\xi=\xi_{\rm out}$) divertor targets.

B. Temperature, density, and velocity distributions

The radial divergence within the SOL of the heat crossing the separatrix from the core into the SOL, $Q_\perp$, enters the SOL-divertor plasma physics calculation directly as a source term in the parallel energy balance equation solved for the heat flux parallel heat flux, Q, in the SOL and divertor in a strip running from the inner divertor target plate around the plasma in a clockwise positive direction to the outer diver plate, as shown in Fig. 2,

$$\frac{dQ}{d\xi}=\frac{Q_\perp}{\Delta_E}-n_z n_e L_z-E_{\rm ion}n_e n_o\langle\sigma v\rangle_{\rm ion}+fI_{\rm ion}n_i n_e\langle\sigma v\rangle_{\rm rec}$$
$$-\frac{3}{2}n_i n_o^c\langle\sigma v\rangle_{\rm cxel}+j_\parallel E_\parallel\equiv\frac{Q_\perp}{\Delta_E}-P_{\rm rad}-P_{\rm at}+P_\Omega, \tag{13}$$

where $Q_\perp/\Delta_E$ is the perpendicular heat flux across the separatrix into the SOL (distributed across a radial energy width Δ_E to take into account the radial transport heat loss), the second term represents impurity radiation (and bremsstrahlung) cooling, and the last three atomic physics terms represent ionization cooling, recombination heating, and charge-exchange plus elastic scattering cooling of the plasma. The sheath boundary conditions specify a heat flux *into* the inner and outer divertor plates

$$Q_{\rm in}=-n_{\rm in}c_{s,{\rm in}}T_{\rm in}\gamma_{\rm in},\quad Q_{\rm out}=n_{\rm out}c_{s,{\rm out}}T_{\rm out}\gamma_{\rm out}, \tag{14}$$

where $\gamma\simeq 6-7$ is the sheath coefficient.

The radial divergence within the SOL of the particle flux directly enters the SOL-divertor plasma physics calculation as a source term in the parallel particle balance equation

$$\frac{d\Gamma}{d\xi}=\frac{\Gamma_\perp}{\Delta_n}+n_e(\nu_{\rm ion}-\nu_{\rm rec})+n_i(\nu_{E_\parallel\times B}+\nu_B+\nu_{\rm dia})+S^{\rm in}_{E_\parallel\times B}, \tag{15}$$

where $\Gamma_\perp$ is the perpendicular particle flux from the core across the separatrix into the SOL (distributed across a radial particle width Δ_n to take into account the radial transport particle loss) represents ionization sources and recombination losses of ions, $\nu_{E\times B}$, ν_B, and $\nu_{\rm dia}$ represent source rates of particles into (+) or out of (−) the SOL-divertor due to radial $E\times B$, grad B, and diamagnetic drifts, and $S^{\rm in}_{E_\parallel\times B}$ represents the source of particles in the inner divertor channel that have $E\times B$ drifted across the private flux region from

the outer divertor channel (for the grad B drift down into the divertor as shown in Fig. 3).

The sheath boundary conditions specify that the particle fluxes into the target plates are

$$\Gamma_{\rm in} = -n_{\rm in}c_{s,\rm in}, \quad \Gamma_{\rm out} = n_{\rm out}c_{s,\rm out}, \tag{16}$$

where c_s is the sound speed. In both Eqs. (14) and (16), the minus sign indicates that the flux is into the plate at the inner divertor target in the negative sense of the parallel coordinate ξ. These incident ions are recycled as neutral atoms and molecules, with the latter being dissociated immediately and transported as low energy atoms until they have a charge-exchange or elastic scattering collision, upon which they are combined with the higher energy reflected neutrals and transported throughout the divertor and SOL and inward across the separatrix.

Solving Eq. (13) for

$$Q(\xi) = -n_{\rm in}c_{s,\rm in}T_{\rm in}\gamma_{\rm in} + \int_{\xi_{\rm in}}^{\xi}\left(\frac{Q_\perp}{\Delta_E} - P_{\rm rad} - P_{\rm at}\right)d\xi', \tag{17}$$

and assuming that parallel heat transport is dominated by classical electron heat conduction $Q(\xi)\approx q(\xi)=-\kappa_0 T^{5/2}dT/d\xi=-\frac{2}{7}\kappa_0 dT^{7/2}/d\xi$ leads to a solution for the temperature distribution in terms of the heat flux calculated from Eq. (17)

$$\begin{aligned} T^{7/2}(\xi) &= T_{\rm in}^{7/2} - \frac{7}{2\kappa_0}\int_{\xi_{\rm in}}^{\xi} Q(\xi')d\xi' \\ &= T_{\rm in}^{7/2} - \frac{7}{2\kappa_0}\int_{\xi_{\rm in}}^{\xi}\left[-n_{\rm in}c_{s,\rm in}T_{\rm in}\gamma_{\rm in} \right. \\ &\quad \left. + \int_{\xi_{\rm in}}^{\xi'}\left(\frac{Q_\perp}{\Delta_E} - P_{\rm rad} - P_{\rm at}\right)d\xi''\right]d\xi'. \end{aligned} \tag{18}$$

The parallel momentum balance equation can be written, neglecting viscosity, as

$$\frac{dM}{d\xi} \equiv \frac{d}{d\xi}(2p + nmv^2) = -m(\nu_{\rm cxel} + \nu_{\rm ion})\Gamma \equiv -m\nu_{\rm mom}\Gamma, \tag{19}$$

where p is the ion pressure, $\nu_{\rm cxel}\equiv n_o(\langle\sigma v\rangle_{\rm cx}+\langle\sigma v\rangle_{\rm el})$ and cx and el refer to charge-exchange and elastic scattering. This equation can be integrated to solve for

$$\begin{aligned} M(\xi) &= M(\xi_{\rm in}) - \int_{\xi_{\rm in}}^{\xi} m\nu_{\rm mom}(\xi')\Gamma(\xi')d\xi' \\ &= 4n_{\rm in}T_{\rm in} - \int_{\xi_{\rm in}}^{\xi} m\nu_{\rm mom}(\xi')\Gamma(\xi')d\xi', \end{aligned} \tag{20}$$

where $M(\xi)$ can then be equated to $(2p+nmv^2)$ to obtain a quadratic equation in $n(\xi)$

$$\begin{aligned} [2p(\xi) + n(\xi)mv^2(\xi)] &\equiv [2n(\xi)T(\xi) + m\Gamma^2(\xi)/n(\xi)] \\ &= M(\xi), \end{aligned} \tag{21}$$

which yields a solution for the plasma ion density

$$n(\xi) = \frac{M(\xi)}{4T(\xi)}[1 \pm \sqrt{1 - 8mT(\xi)\Gamma^2(\xi)/M^2(\xi)}] \tag{22}$$

that can be used in the definition of Γ to obtain the plasma flow velocity

$$v(\xi) = \Gamma(\xi)/n(\xi). \tag{23}$$

The sheath boundary condition on the parallel flow velocity into the target plate is

$$v(\xi_{\rm in}) = -c_{s,\rm in} \equiv -\sqrt{\frac{2T_{\rm in}}{m}}, \quad v(\xi_{\rm out}) = c_{s,\rm out} \equiv \sqrt{\frac{2T_{\rm out}}{m}}. \tag{24}$$

In all calculations to date, the larger value obtained using the + sign in Eq. (22) has been of the magnitude observed in experiment.

C. Electrostatic potential

Integrating the electron momentum balance yields an expression for the electrostatic potential that explicitly accounts for impurities

$$\begin{aligned} \phi(\xi) &= \phi_{\rm in} + \frac{[1 + c_e^{(2)}\beta/z_{\rm eff}]}{e}[T(\xi) - T_{\rm in}] \\ &\quad + \int_{\xi_{\rm in}}^{\xi}\frac{T(\xi')}{en(\xi')}\frac{dn(\xi')}{d\xi'}d\xi' - \int_{\xi_{\rm in}}^{\xi}\frac{\beta\eta_\parallel}{z_{\rm eff}}j_\parallel(\xi')d\xi', \end{aligned} \tag{25}$$

where

$$\beta = \frac{1 + \Sigma_k n_k z_k^2/n_i}{1 + \Sigma_k n_k z_k/n_i}$$

and $\phi_{\rm in}$ ($\phi_{\rm out}$) is the potential just in front of the inner (outer) divertor plate, which is related to the current into the inner (outer) divertor plate $j_{\rm pl}^{\rm in}$ ($j_{\rm pl}^{\rm out}$) by the sheath current-potential relation

$$\begin{aligned} \phi_{\rm in} &= -\frac{T_{\rm in}}{e}\ln\left[\frac{\sqrt{m_i/\pi m_e}(1-\delta)}{1 - j_{\rm pl}^{\rm in}/n_{\rm in}ec_{si,\rm in}}\right], \\ \phi_{\rm out} &= -\frac{T_{\rm out}}{e}\ln\left[\frac{\sqrt{m_i/\pi m_e}(1-\delta)}{1 - j_{\rm pl}^{\rm out}/n_{\rm out}ec_{si,\rm out}}\right], \end{aligned} \tag{26}$$

where $\sigma_\parallel = 2n_e e^2\tau_e/m_e$, $\tau_e = 3\sqrt{m_e}T^{3/2}/4\sqrt{2\pi}n_e \ln\Lambda e^4$, and δ is the secondary electron emission coefficient.

D. Parallel current

The net current density into the target plates is given by the sum of the ion current density nec_{si} and the electron current density, $\frac{1}{4}n(-e)\bar{c}_e e^{e\phi/T}$ for a Maxwellian distribution,

$$j_{\rm pl}^{\rm in} = ne\left[c_{si} - \tfrac{1}{4}\bar{c}_e e^{e\phi/T_e}\right], \tag{27}$$

where $\bar{c}_e = (8T_e/\pi m_e)^{1/2}$ is the average electron speed for a Maxwellian distribution.

The current density must be divergence-free

$$\nabla \cdot \mathbf{j} \equiv \frac{dj_{\parallel}}{d\xi} + \frac{dj_{\perp}}{d\ell_{\perp}} + \frac{dj_r}{dr} = 0, \tag{28}$$

which may be solved for the parallel current produced by radial drift currents into or out of the SOL

$$j_{\parallel}(\xi) = -j_{\mathrm{pl}}^{\mathrm{in}} - \int_{\xi_{\mathrm{in}}}^{\xi} \left[\frac{dj_{\perp}}{d\ell_{\perp}} + \frac{dj_r}{dr} \right] d\xi'. \tag{29}$$

The minus sign in front of the first term on the right results from the fact that Eq. (27) specifies the current into the inner divertor plate, while the positive sense of the current in this model is out of the inner divertor plate (but into the outer divertor plate); i.e., $j_{\parallel}(\xi_{\mathrm{in}}) = -j_{\mathrm{pl}}^{\mathrm{in}}$.

These cross-field currents are driven by grad B and curvature drifts, as discussed in Sec. III E. To leading order (neglecting possible finite-Larmor-radius effects), they are not driven by $E \times B$ drifts, which are the same for ions and electrons and hence do not produce currents. The diamagnetic currents have been shown to be almost divergence-free,[11] except for small terms related to the nonuniformity in B, which are treated in terms of the grad B and curvature drifts. The divergent part of the diamagnetic current has been shown to correspond to the vertical drift current due to grad B and curvature.[11] Cross-field currents also may be driven by cross-field transport, viscosity, and other mechanisms that have different effects on ions and electrons, but these mechanisms have been found[10,11] to provide smaller contributions and are not considered at present.

E. grad *B* and curvature drifts

The grad B and curvature drifts are

$$\begin{aligned} v_{\nabla B} &= \frac{T}{e} \frac{\mathbf{B} \times \nabla B}{B^3} \approx \frac{T}{eRB} \mathbf{n}_z, \\ v_c &= -\frac{m v_{\parallel}^2}{e} \frac{\mathbf{B} \times \mathbf{R}}{B^2 R^2} \approx \frac{m v_{\parallel}^2}{eRB} \mathbf{n}_z, \\ v_B &\equiv v_{\nabla B} + v_c \approx \frac{3T}{eRB} \mathbf{n}_z, \end{aligned} \tag{30}$$

where $\mathbf{n}_z$ is a unit vector in the vertical direction, up or down depending on the direction of $\mathbf{B}$, and $v_{\parallel} \approx v_{\mathrm{th}}$. The drifts are in opposite directions for ions and electrons because of the charge sign difference, producing a current

$$\mathbf{j}_B = 2ne\mathbf{v}_B \approx \frac{6nT}{BR} \mathbf{n}_z. \tag{31}$$

For the configuration in Figs. 2 and 3, the vertical unit vector $\mathbf{n}_z$ is directed downward. Thus, the radial drift currents are radially inward from the SOL into the core in the upper hemisphere ($0 \le \theta \le \pi$) and radially outward from the core into the SOL in the lower hemisphere ($\pi \le \theta \le 2\pi$), as indicated in Fig. 3.

The ion grad B and curvature drifts also produce a poloidal particle drift which, when mapped onto the pseudoparallel coordinate (see discussion at beginning of section), is

$$\Gamma_{\nabla B}^{\parallel} = (\mathbf{n}_{\parallel} \cdot \mathbf{n}_z) \Gamma_{\nabla B}^{z} = \left(\frac{B_{\theta}}{B} \cos\theta \right) \frac{3nT}{eBR}, \tag{32}$$

which is downward in both the inner and outer SOLs and divertors, as indicated in Fig. 3. Here, the angle θ is with respect to the outboard midplane. In the divertor, $\cos\theta$ is replaced by $\sin\alpha$, where α is the angle of incidence with respect to the horizontal of the separatrix, as illustrated in Fig. 3.

F. Diamagnetic drifts

It may seem strange that diamagnetic drifts are not explicitly included in the calculation since the leading order local force balance on the plasma balances the pressure gradient with a $V \times B$ force, which drives diamagnetic drift velocities orthogonal both to the field and the pressure gradient. In particular, a radial diamagnetic flow is driven by the pressure gradient in the direction perpendicular to the 2D strip in which the transport calculation of this paper is being carried out

$$v_{\mathrm{dia}}^{r} = \frac{-1}{neB} \frac{\partial p}{\partial \ell_{\perp}} \simeq \frac{-1}{neB} \frac{\partial p}{\partial \ell_{\theta}} \simeq \frac{-1}{neB} \frac{B}{B_{\theta}} \frac{\partial p}{\partial \xi}. \tag{33}$$

The radial pressure gradient also drives a diamagnetic drift velocity in the direction perpendicular to the 2D strip along the field lines.

However, the diamagnetic drift contributions to the plasma current and particle flux are divergence-free except for small terms associated with the field nonuniformity, and the nonvanishing diamagnetic terms are just the grad B (and curvature) current and particle drift contributions already included in the calculation.[11] In other words, the surviving terms in the diamagnetic drift enter the calculation through the grad B drifts described above, and there is not an additional explicit diamagnetic drift contribution to either the parallel current or the particle sinks and sources in this calculation.

G. *E*×*B* drifts

$E \times B$ drifts do not produce currents, but they do produce particle flows. The poloidal variation in the electrostatic potential produces a vertically directed electric field and a corresponding "radial" $E \times B$ drift. This electric field is $\mathbf{E} = -\nabla\phi$, which, in general, has poloidal and radial components. We estimate this poloidal electric field and the resulting radial drift as

$$E_{\parallel} = -\left(\frac{d\phi}{d\ell_{\theta}} \right) \approx -\left(\frac{d\phi}{d\xi} \right), \quad v_{E_{\parallel} \times B}^{r} = \frac{\mathbf{E} \times \mathbf{B}}{B^2} = \frac{-\dfrac{d\phi}{d\xi}}{B}. \tag{34}$$

Note that this electric field is in the poloidal direction, and the "parallel" subscript indicates that it is calculated by taking the potential gradient with respect to the pseudoparallel coordinate system.

The radial $E \times B$ flows from the outboard divertor channel into the private flux region and from the private flux

region into the inboard divertor channel will transfer ions from the outboard divertor channel across the private flux region beneath the plasma to the inboard divertor channel.

The "radial drift" loss or gain of ions from both the SOL and the divertor channels can be represented by an $E\times B$ loss frequency

$$\nu_{E_\parallel\times B}(\xi)=\frac{v^r_{E_\parallel\times B}(\xi)}{\varepsilon\Delta_n}, \tag{35}$$

where Δ_n is an estimate of the "radial width" of the SOL calculated as discussed for Eq. (6) and $\varepsilon\approx 3$ is a flux surface expansion factor taking into account the widening of the SOL into the divertor channel. (The grad B and diamagnetic drift loss/gain frequencies are calculated in a similar way.) Assuming that some fraction $f_{E\times B}$ of the ions lost into the private flux region from the outboard divertor channel flow into the inboard divertor channel, the source density of ions to the inboard divertor channel may be represented

$$S^{\rm in}_{E_\parallel\times B}=\frac{f_{E\times B}\int_{\xi_{\rm out}}^{\xi_{X_{\rm out}}}\nu_{E_\parallel\times B}(\xi)n(\xi)d\xi}{\int_{\xi_{\rm in}}^{\xi_{X_{\rm in}}}d\xi}, \tag{36}$$

where $\xi_{X_{\rm out,in}}$ denotes the location of the X point in the outer, inner SOL-divertor.

There is a radially outward directed electric field in the SOL produced by the radial temperature gradient in the SOL

$$E_r(\xi)=\frac{-d\phi}{dr}=-\phi\left(\frac{1}{\phi}\frac{d\phi}{dr}\right)\simeq-\phi\left(\frac{1}{T}\frac{dT}{dr}\right)\equiv\phi\Delta_T^{-1}, \tag{37}$$

which produces poloidal clockwise $E\times B$ drifts and particle fluxes in the SOL

$$v^\theta_{E_r\times B}(\xi)=\frac{\phi(\xi)\Delta_T^{-1}}{B},\quad \Gamma^\theta_{E_r\times B}(\xi)=\frac{n(\xi)\phi(\xi)\Delta_T^{-1}}{B}. \tag{38}$$

The component of this poloidal particle flux parallel to the field in the SOL constitutes a parallel drift particle flux

$$\Gamma^\parallel_{E_r\times B}(\xi)=\frac{B_\theta}{B}\Gamma^\theta_{E_r\times B}(\xi)=\frac{n(\xi)\phi(\xi)\Delta_T^{-1}B_\theta}{B^2}, \tag{39}$$

which circulates clockwise around the SOL.

Both the parallel particle drift fluxes [Eqs. (32) and (39)] are additive to the particle flux due to particle sources calculated from Eq. (15).

H. Total parallel ion flux

The total parallel ion flux is calculated by integrating the particle balance Eq. (15), including the radial transport and radial drift losses and sources, and adding the poloidal grad B and $E\times B$ drift fluxes mapped onto the parallel coordinate

$$\Gamma(\xi)=\Gamma_{\rm in}+\int_{\xi_{\rm in}}^{\xi}\left[\frac{\Gamma^{\rm sep}_\perp}{\Delta_n}+n_e(\nu_{\rm ion}-\nu_{\rm rec})+n_i(\nu_{E_\parallel\times B}+\nu_B+\nu_{\rm dia})+S^{\rm in}_{E_\parallel\times B}\right]d\xi'+\Gamma^\parallel_{\nabla B}(\xi)+\Gamma^\parallel_{E_r\times B}(\xi) \tag{40}$$

with $\Gamma_{\rm in}$ given by the sheath boundary condition of Eq. (16) at the inner divertor target.

I. Solution procedure

The coupled set of nonlinear equations described above [Eqs. (17), (18), (20), (22), (23), (25), and (29)–(40)] are solved numerically using iterative procedures, the convergence of which is a somewhat delicate process. This solution procedure is incorporated in an integrated modeling code[12] which solves the core plasma power and particle balances to calculate the particle and heat fluxes $(\Gamma^{\rm sep}_\perp, Q^{\rm sep}_\perp)$ flowing across the separatrix from the core into the SOL, the two-point equations for the divertor and SOL which provides the background plasma parameters for the neutral calculation, and the 2D transport of recycling neutrals. This calculation also provides starting conditions for the iterative solution.

J. Summary of physics model

The physics model builds upon what was learned in the pioneering work of Rognlien *et al.*[10] and Rozhansky *et al.*[11] to solve the particle, momentum, and energy balance equations and the current continuity equation. The analytical Miller equilibrium[7] is introduce to eliminate the need for coupled MHD equilibrium calculations. A computationally economical integral neutral transport model[12] (instead of a computationally intensive Monte Carlo neutrals calculation) is utilized. The Keilhacker[13] model is used to treat parallel impurity transport. Some approximations for radial transport based on experimental observation are made. An iterative solution procedure is used to integrate the resulting set of coupled, nonlinear ordinary differential equations. This results in a computationally tractable calculation that provides a solution in minutes on a modern PC.

IV. EFFECTS OF POLOIDAL-DEPENDENT HEAT AND PARTICLE FLUXES FROM THE CORE ON THE DIVERTOR-SOL PLASMA DISTRIBUTIONS

A. Model problem

In order to ensure a realistic plasma edge regime, a model problem was chosen which had machine and plasma core parameters of a DIII-D H-mode discharge, with two exceptions. The two divertor legs were symmetrized (i.e., made more like Figs. 2 and 3 than the more asymmetric divertor configuration actually found in DIII-D) in order to avoid geometrical asymmetries that would otherwise additionally complicate the interpretation of the results of the calculations. In such a model problem, the solution in the absence of drifts should be in-out symmetric. Second, the D shape of the plasma was not retained in modeling the essentially vertical grad B and curvature drifts, with the effect of

making the radial and poloidal (parallel) components of these drifts of symmetric magnitude in the inner and outer SOL.

The model (R=1.7 m, a=0.6 m, κ=1.8, B=2.0 T, I=1.2 MA, q_{95}=4) represented a lower single null divertor plasma with the toroidal field such that the grad B ion drift was down into the divertor, i.e., the configuration illustrated in Figs. 2 and 3. The magnitude of the power and particle fluxes into the SOL from the core plasma were calculated to match experimental conditions for this H-mode discharge. Two SOL-divertor plasma calculations were made using the equations of Sec. II. In the first calculation the power and heat fluxes into the SOL were represented as uniformly distributed. In the second calculation, these fluxes were distributed as specified by the factor $H(r,\theta)$ in Eq. (12).

The equations of Sec. II were numerically integrated over a grid structure along the field lines from the inner to the outer divertor plates. A small (5 cm in the parallel dimension, about 1 cm in the poloidal dimension normal to the target plates) recycling region in front of each divertor plate, a prerecycling region of twice that length, and eight other regions represented each divertor channel up to and including the X-point region (total length of each 2.95 m along field lines). The SOL plasma from inner to outer X points (parallel distance of 53.02 m) was divided into 30 equal regions. With reference to Fig. 2, the recycling regions are 1 and 50, the inner and outer X points are in regions 10 and 41, the inner and outer midplanes are in regions 18 and 33, and the "crown" at the top is regions 25 and 26. The interfaces bounding region n are n to the left and "n+1" to the right. The symmetry point is interface 26 between regions 25 and 26. With the numerical integration scheme employed in this paper, all quantities were calculated at the 51 region interfaces, and average values over each region were constructed for evaluation of integrals. All results will be plotted against interface number.

Particle sources were treated as follows. The gas fueling source for the deuterium (1.5×10^{20} #/s into the upper outboard plasma chamber) was represented explicitly, and the resulting neutral atoms were transported[12] through the edge region across the separatrix to fuel the core plasma. An average ion flux of $\Gamma_\perp=1.6\times10^{20}$ #/m^2 s from the core plasma into the SOL was calculated, taking into account this neutral influx into the core, but consisting mostly of ions produced by the neutral beam particle source. The deuterium ions striking the target plates (consisting both of ions crossing the separatrix from the core and ions produced by ionization of neutral atoms in the SOL and divertor) were reflected as neutral atoms at about one-half their incident energy or re-emitted as molecules which were dissociated into 2 eV atoms in the recycling regions 1 and 50 and were then transported throughout the edge region until ionized in the divertor, SOL or plasma edge inside the separatrix.

Two impurity ion species were modeled:[13] carbon, which is an intrinsic impurity, and argon which is sometimes used to enhance radiation. The carbon source was the calculated sputtering of the deuterium ions incident on the divertor target plates and was distributed over the first two regions (i.e., 1 and 2, 49 and 50) in front of the target. Carbon was transported as a single ion species with an average charge state that varied with local electron temperature along the field lines. Carbon ions returning to the target plates were reflected with a coefficient R=0.99, which included in an approximate manner also the effects of carbon self-sputtering. An argon source of 2×10^{19} #/s injected in the private flux region was assumed to be pumped by the divertor plasma and was represented as a uniformly distributed particle source in the two divertor plasmas (regions 1–9 and 42–50). The argon ions incident on the divertor targets were reflected with coefficient R=0.99.

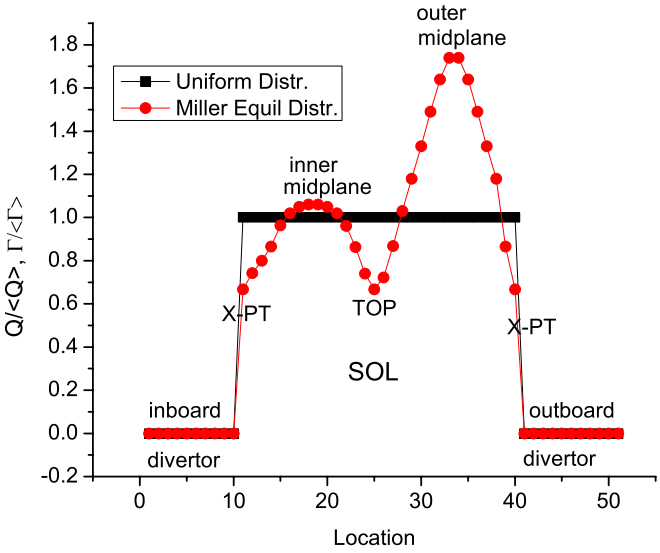

FIG. 4. (Color online) Poloidal distribution of power and particle fluxes into SOL.

An average heat flux of $Q_\perp=8.8\times10^4$ W/m^2 into the SOL from the core plasma was calculated from a core power balance, taking into account the 4.9 MW neutral beam heating, the small Ohmic heating, and the radiation from inside the separatrix. Radial transport was represented by a gradient scale length of 2 cm for density and temperature.

B. Poloidal distribution of power and particle fluxes

The factor $H(r,\theta)$ in Eq. (12) and the corresponding uniform distribution are shown in Fig. 4. The outward peaking is due to the compression of flux surfaces on the outboard, and the minima at the top and bottom reflect the expansion of the elongated flux surfaces in these regions. Two calculations were made, one using $H(r,\theta)$ to distribute both the power and particle influxes from the core into the SOL, and the second using $H(r,\theta)$ to distribute only the power influx and leaving the particle influx uniform. There were only slight differences between the results of these two calculations, indicating that it is the poloidal distribution of the power influx that causes the calculated differences between the uniform and $H(r,\theta)$ influx distributions that will be shown.

C. Density and temperature

The calculated ion density and temperature parallel profiles in the divertor and SOL are shown in Figs. 5 and 6. The effect of the outboard peaked power and particle influx profiles shown in Fig. 4 is to increase the temperature and de-

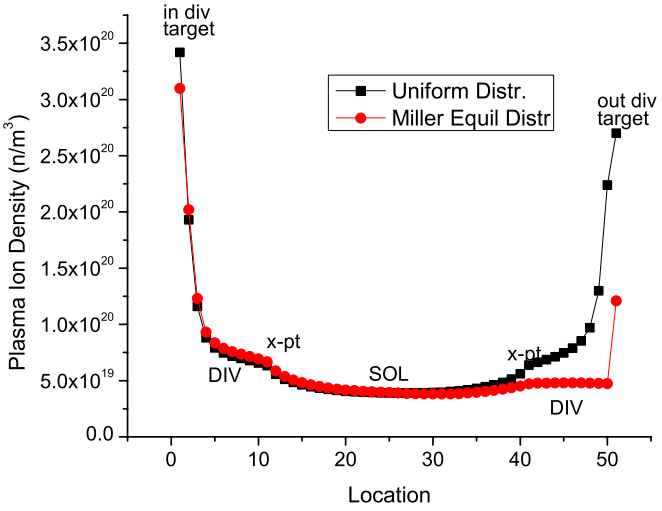

FIG. 5. (Color online) Ion density profile in SOL divertor.

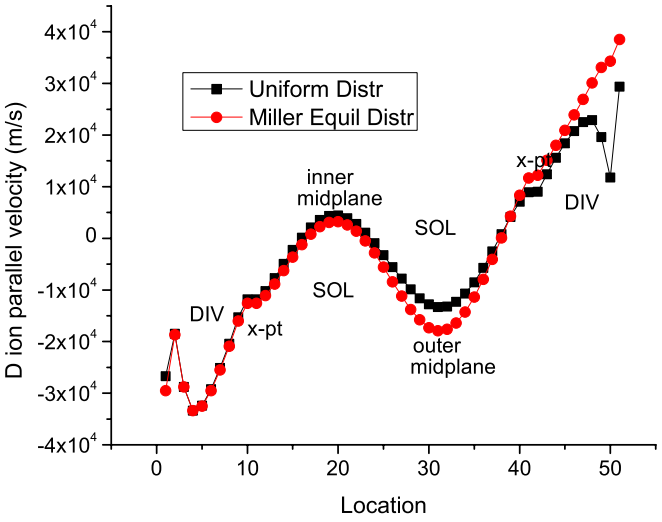

FIG. 7. (Color online) Ion parallel flow velocity distribution.

crease the density in the outboard divertor relative to the inboard divertor. This is consistent with the usual experimental observation in DIII-D that the inboard divertor is cooler (and frequently detached) than the outboard divertor. These calculations are suggestive that this observed phenomenon is due, at least in part, to the distribution of the power and particle fluxes from the core into the SOL. The recycling neutral density is quite large just in front of the divertor plates, accounting for the sharp drop in temperature and increase in density calculated in this location.

As a reference point, when these same calculations are performed with a uniform power and particle influx and without the drifts, the distribution is close to the uniform distributions shown in Figs. 5 and 6, but are in-out symmetric. So, the asymmetry of the "uniform distr" is due to the drifts, and the further asymmetry of the "Miller equil distr" is due to the poloidal distribution of the heat and particle influx shown in Fig. 4.

These results, which included neutrals, impurities, and the effect of $E\times B$ and grad B drifts, are consistent with previous calculations[2] of the effect of the poloidal dependence of the particle and power influx into the SOL on the in-out power asymmetry in the asymmetric divertor experiment upgrade (ASDEX-U) even though the latter calculations were made without taking the effect of drifts into account.

D. Parallel flow velocity and current

The deuterium ion parallel flow velocity and the parallel current density distributions are relatively insensitive to the poloidal distribution of the power and particle fluxes into the SOL from the core, as shown in Figs. 7 and 8.

The interesting result of multiple flow stagnation points, caused by the poloidal distribution of particles sources and sinks in the SOL due to radial drifts across the separatrix, has been experimentally observed.[14] The variation in the parallel current distribution, due to the current continuity requirement and the distribution of the radial grad B current into the SOL in the upper hemisphere and out of the SOL in the lower hemisphere (see Fig. 3), is shown in Fig. 8.

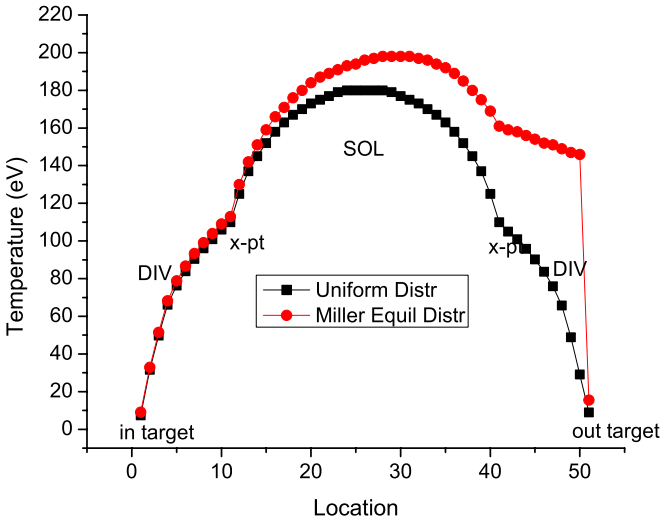

FIG. 6. (Color online) Temperature profile in SOL divertor.

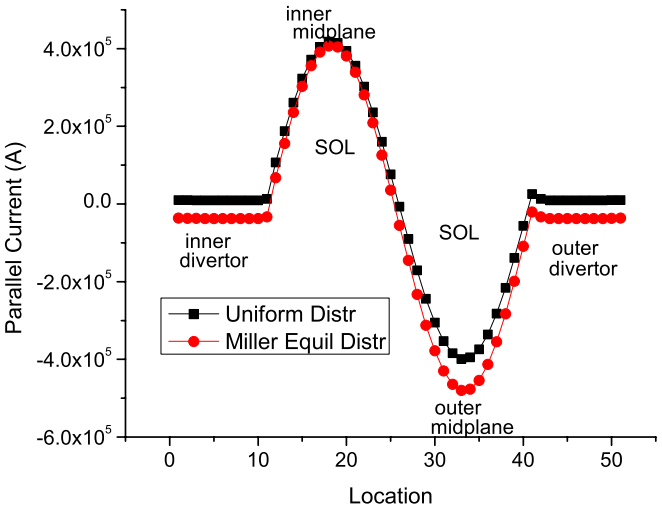

FIG. 8. (Color online) Parallel current distribution.

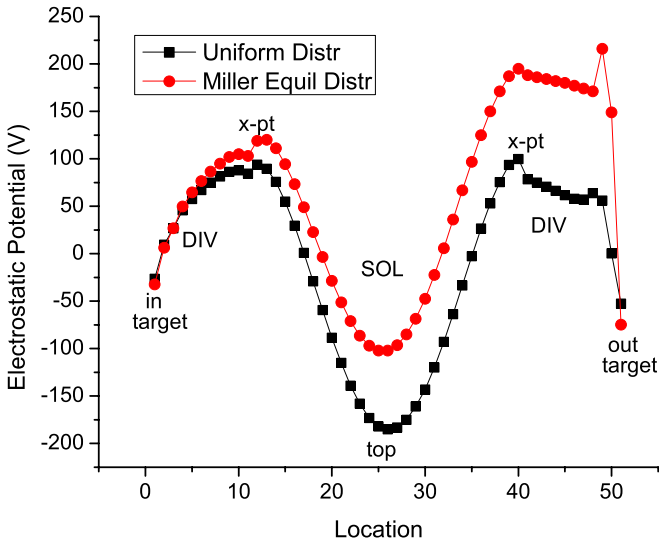

FIG. 9. (Color online) Electrostatic potential distribution.

E. Electrostatic potential

Taking the poloidal distribution of power and particle fluxes into account does affect the calculation of the electrostatic potential distribution, as indicated in Fig. 9. The increase in temperature in the outboard divertor caused by the outboard peaking of the power and particle fluxes in the Miller equilibrium accounts for much of the increase in electrostatic potential in the outboard divertor for that case, but the increase in potential also in the top and inboard SOL is due to other factors in Eq. (25).

V. SUMMARY

The parallel distribution of ion density, temperature, parallel ion flow velocity, parallel current, and electrostatic potential in the SOL and divertor of a DIII-D tokamak model problem has been calculated for (i) a poloidally uniform distribution of the particle and power fluxes from the core plasma into the SOL and for (ii) a poloidally nonuniform distribution of particle and power fluxes proportional to the poloidal distribution of radial gradients (i.e., inversely proportional to the spacing between flux surfaces). These calculations took into account neutrals, impurities, and the effect of $E \times B$ and grad B (diamagnetic) drifts. Perhaps the most important result of the calculations was the confirmation in the presence of drifts that the larger power and particle fluxes from the core plasma to the outboard than to the inboard SOL could contribute to producing the observed in-out divertor power asymmetry in DIII-D and ASDEX-U by producing a larger temperature in the outboard than the inboard divertor. Significant quantitative effects on the particle flow velocity, the parallel current, and the electrostatic potential were found when the poloidal distribution of power and particle fluxes to the SOL were taken into account.

ACKNOWLEDGMENT

The reviewer's comments have been quite useful in better putting the results of the paper into perspective vis-à-vis related work.

[1] V. Kotov, D. Reiter, R. A. Pitts, S. Jachmich, A. Huber, D. P. Coster, and JET/EFDA Team, Plasma Phys. Controlled Fusion **50**, 105012 (2008).
[2] D. P. Coster, J. W. Kim, Y. Nishimura, R. Schneider, X. Bonin, V. Rozhansky, and S. Voskoboynikov, Plasma Phys. Controlled Fusion **44**, 979 (2002).
[3] W. M. Stacey and R. J. Groebner, Phys. Plasmas **14**, 012501 (2007).
[4] J. Luxon, Nucl. Fusion **42**, 614 (2002).
[5] W. M. Stacey, Contrib. Plasma Phys. **48**, 94 (2008).
[6] W. M. Stacey and R. J. Groebner, Phys. Plasmas **13**, 012513 (2006).
[7] R. L. Miller, M. S. Chu, J. M. Greene, Y. R. Lin-Liu, and R. E. Waltz, Phys. Plasmas **5**, 973 (1998).
[8] S. J. Zweben, J. A. Boedo, O. Grulke, C. Hidalgo, B. LaBombard, R. J. Maqeda, P. Scarin, and J. L. Terry, Plasma Phys. Controlled Fusion **49**, S1 (2007).
[9] W. M. Stacey, Phys. Plasmas **15**, 122505 (2008).
[10] T. D. Rognlien, D. D. Ryutov, N. Mattor, and G. D. Porter, Phys. Plasmas **6**, 1851 (1999); T. D. Rognlien and D. D. Ryutov, Contrib. Plasma Phys. **38**, 152 (1998); T. D. Rognlien, Plasma Phys. Controlled Fusion **47**, A283 (2005).
[11] V. A. Rozhansky, S. P. Voskoboynikov, E. G. Kaveeva, D. P. Coster, and R. Schneider, Nucl. Fusion **41**, 387 (2001); **42**, 1110 (2002); **43**, 614 (2003); V. A. Rozhansky, Contrib. Plasma Phys. **46**, 575 (2006).
[12] W. M. Stacey, Phys. Plasmas **5**, 1015 (1998); Nucl. Fusion **40**, 965 (2000).
[13] M. Keilhacker, R. Simonini, A. Taroni, and M. Watkins, Nucl. Fusion **31**, 535 (1991).
[14] M. Groth, G. D. Porter, J. A. Boedo *et al.*, "Measurements and simulations of main scrape-off layer flows in DIII-D," Proceeding of the Plasma Surface Interaction Conference, Toledo, 2008 [J. Nucl. Mater. (to be published)].